

Emplacement Conditions and Vent Locations for the Channelized and Partially Buried Lava Flows Southwest of Arsia Mons

Flynn I.T.W.¹, Crown, D.A.² and Ramsey, M.S.¹, ¹Department of Geology and Environmental Science, University of Pittsburgh, Pittsburgh, PA 15260, itf2@pitt.edu; ²Planetary Science Institute, Tucson, AZ 85719



Introduction

Channelized lava flows are commonly observed in the major volcanic provinces on Mars. The morphology of these flows indicate specific emplacement conditions, which can be modeled to determine flow parameters such as effusion rate, emplacement duration, yield strength, and viscosity [1-4]. However, most channelized flows are only partially exposed due to younger overlapping flows or aeolian mantling. This is seen extensively throughout the lava flow field south of Arsia Mons [5]. Models that rely upon the visible extent of a flow can provide useful insights, but those results could easily misrepresent the true flow conditions at the time of emplacement.

In this study, we present an application of the PyFLOWGO thermorheological model, developed for terrestrial applications and modified for Mars conditions. The goal is to determine the emplacement and flow parameters for a series of the Arsia Mons channelized flows whose aerial extents are not completely visible (Fig. 1). Applying the model in a novel way to constrain channel width rather than the exposed channel length also provides the capability to estimate the original channel length. We can then project this length upslope to search for potential vent locations.

Data & Methods

The application of PyFLOWGO to Mars channelized lava flows presented here has two steps. For both, the starting assumed rheological parameters are taken from the 2012-13 Tolbachik eruption, which represents a typical basaltic composition [6]. Adaptation of PyFLOWGO to Mars follows methods from [7] but with minor improvements. All modeling was performed over a constant slope of 2° which is representative of the region.

Measurements of channel width, flow width, and length of the channelized zone for each flow were made using the Context Camera (CTX) (~6 m/pixel). Initial channel depth was measured using the MOLA Precision Experiment Data Point Records (PEDR (~160 m spot size, ~300 m along track spacing and 37 cm effective vertical resolution)). The "starting" (first visible evidence) channel width and depth measurements are necessary to initiate the PyFLOWGO model. Central channel width measurements were taken every 1000 m downflow to corroborate the results as the model propagates the flow downslope.

- **Step 1.** We first vary three of the model inputs (eruption temperature, starting crystal fraction, and crystals grown during cooling) within reasonable ranges to match the exposed channel length to within <5% [8].
- **Step 2.** We then use the rheological parameters determined from Step 1 and iteratively narrow the initial channel width assuming narrowing of the channel closer to the source [9-11]. This step is considered complete where the modeled channel width matches the distal channel width also to within <5%. This modeling step yields an estimated total channel length of the flow. This length is then projected upslope, following the regional aspect and generated slope vectors to a potential vent location. Slope vectors were generated in ArcGIS v10.8 using the MOLA/HRSC blended DEM.

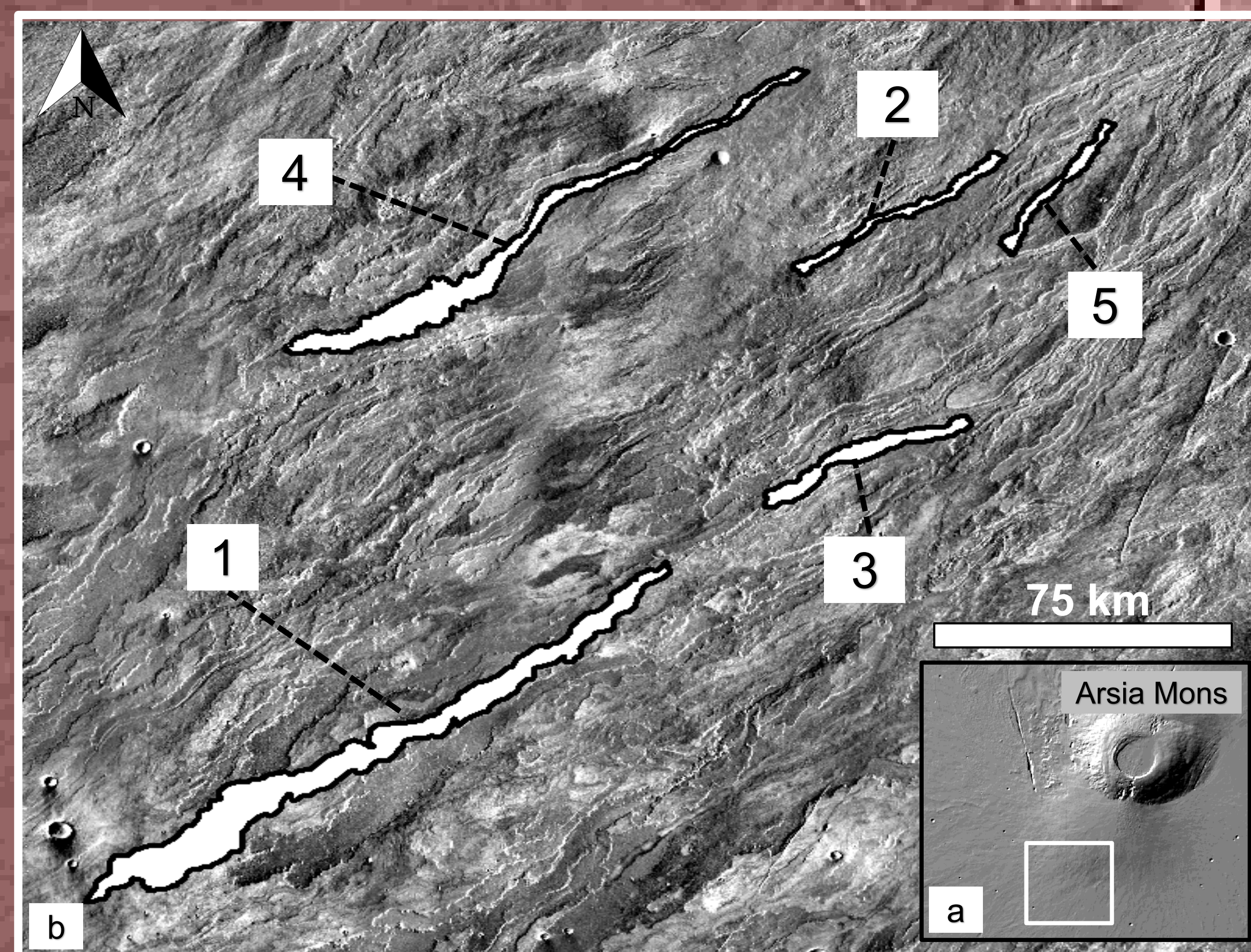


Figure 1. (a) Shaded relief map derived from the Mars Orbiter Laser Altimeter (MOLA) / High Resolution Stereo Camera (HRSC) blended digital elevation model (DEM) dataset (~200 m/pixel; ± 3 m vertical resolution), showing the southern Tharsis Montes volcanic region and the study area, outlined by the white box (14-20.5°S, 122.5-128.4°E). There are ~21 lava flows with well defined central channels in the study area; we chose five representative flows based on size, areal distribution, and central channel development. (b) THEMIS day TIR mosaic (100m/pixel) of the five flows, outlined and numbered.

	Effusion Rate (m ³ s ⁻¹)	Viscosity (Pa s)	Yield Strength (Pa)
Flow 1	5.40 x 10 ³ ± 300	6.70 x 10 ⁵	381
Flow 2	6.25 x 10 ³ ± 250	2.85 x 10 ⁵	124
Flow 3	2.50 x 10 ³ ± 150	2.84 x 10 ⁵	124
Flow 4	3.90 x 10 ³ ± 150	6.15 x 10 ⁵	352
Flow 5	6.75 x 10 ³ ± 200	2.14 x 10 ⁵	66

Table 1. Best-fit PyFLOWGO model results for effusion rate, viscosity, and yield strength for the five flows modeled. Viscosity and yield strength values reflect conditions when the flow has ceased moving.

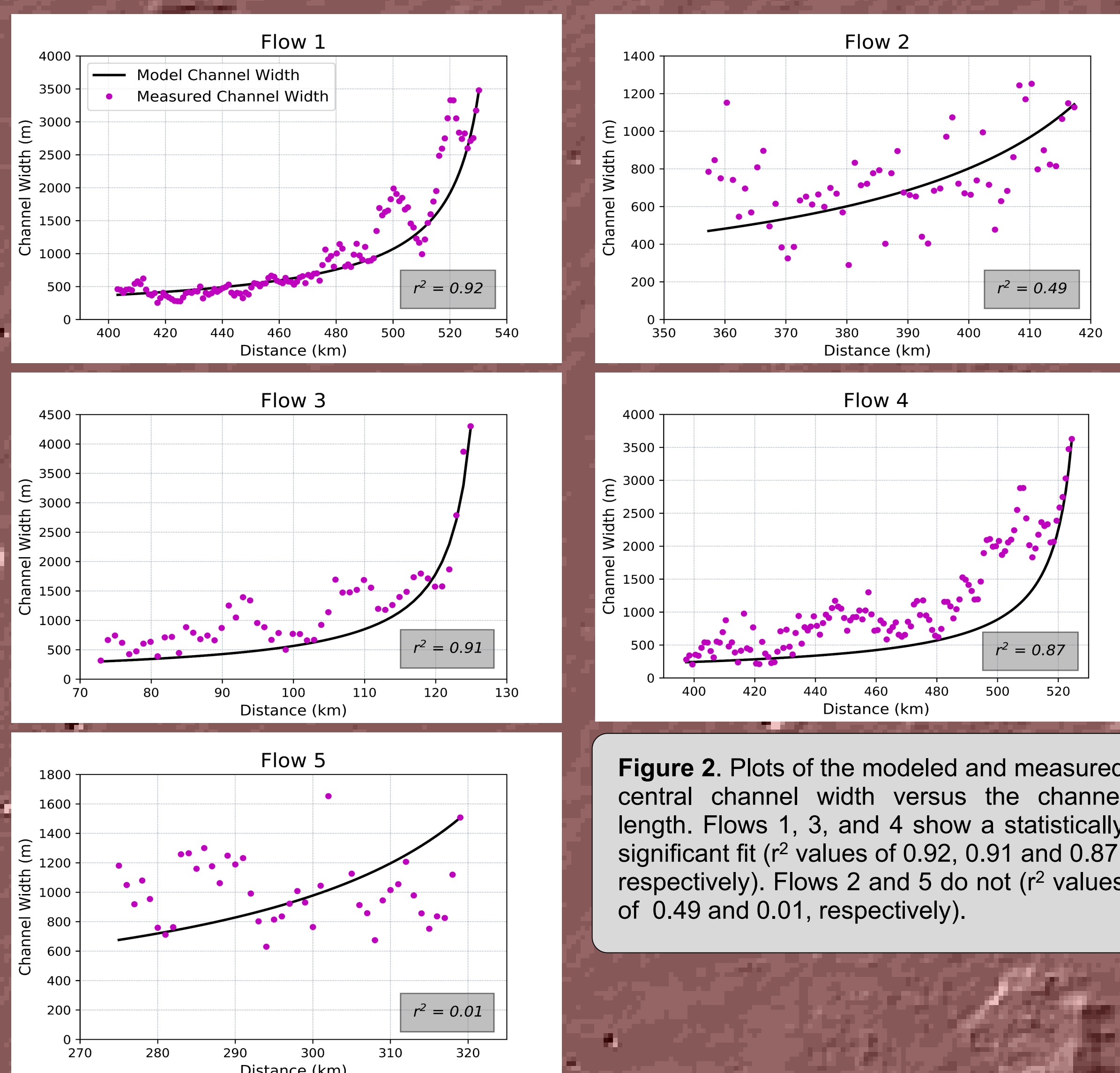


Figure 2. Plots of the modeled and measured central channel width versus the channel length. Flows 1, 3, and 4 show a statistically significant fit (r^2 values of 0.92, 0.91 and 0.87, respectively). Flows 2 and 5 do not (r^2 values of 0.49 and 0.01, respectively).

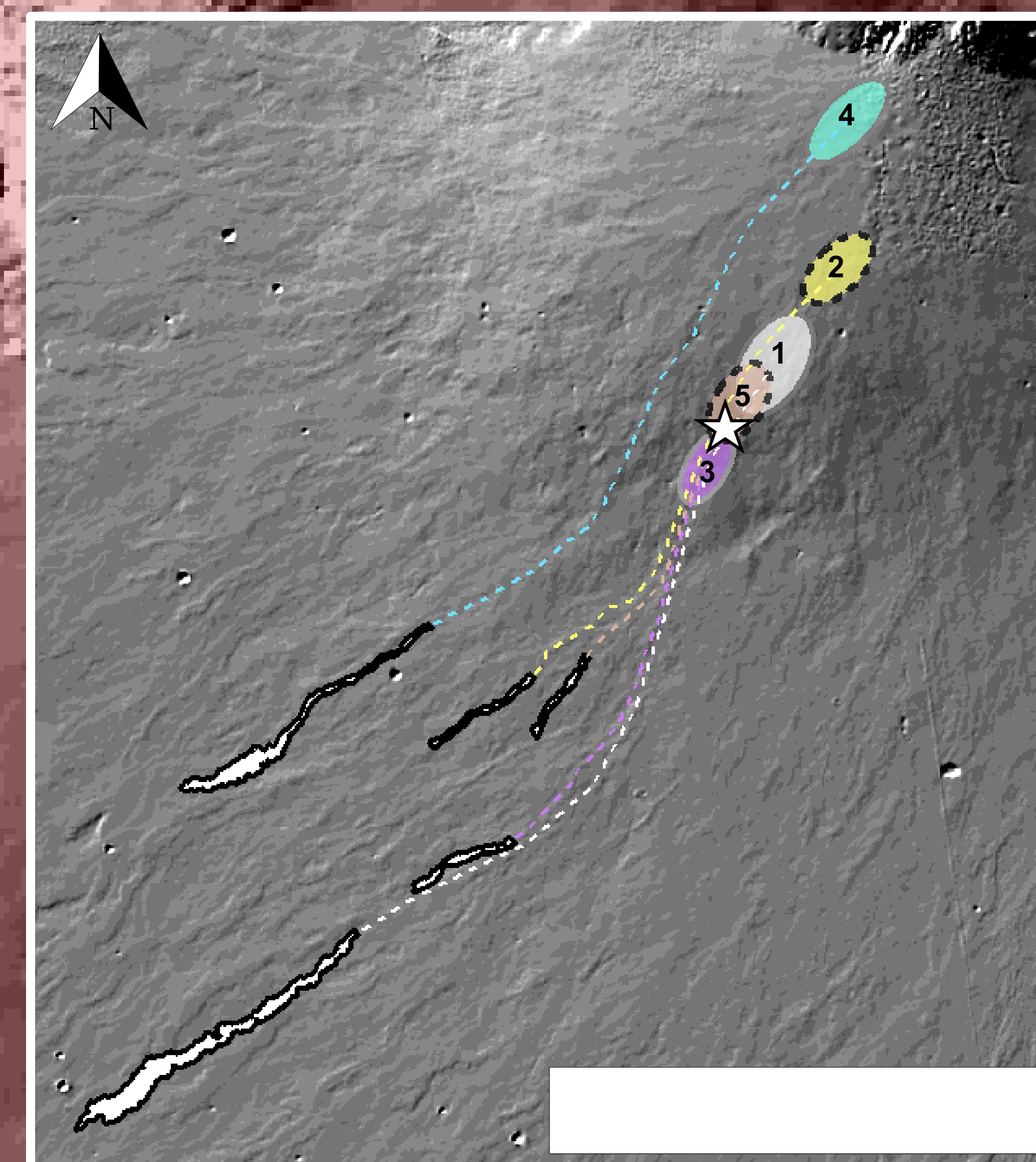


Figure 3. The five flows of the study with the back projected tracks shown by dashed lines. Back projection is done by using a 2° slope and following the regional aspect and slope vectors. Colored ellipses represent the error range associated with the CTX and MOLA measurements (channel width and initial channel depth). The dashed line around the ellipses for Flows 2 and 5 indicate the increased uncertainty in those results based on our initial modeling (Figure 5). Flows 1, 3 and 5 (and possibly 2) cluster together in the same region, whereas Flow 4 projects back to a different area. White star shows the location of the possible vent source (Figure 4). Base image is MOLA/HRSC blended DEM hillshade.

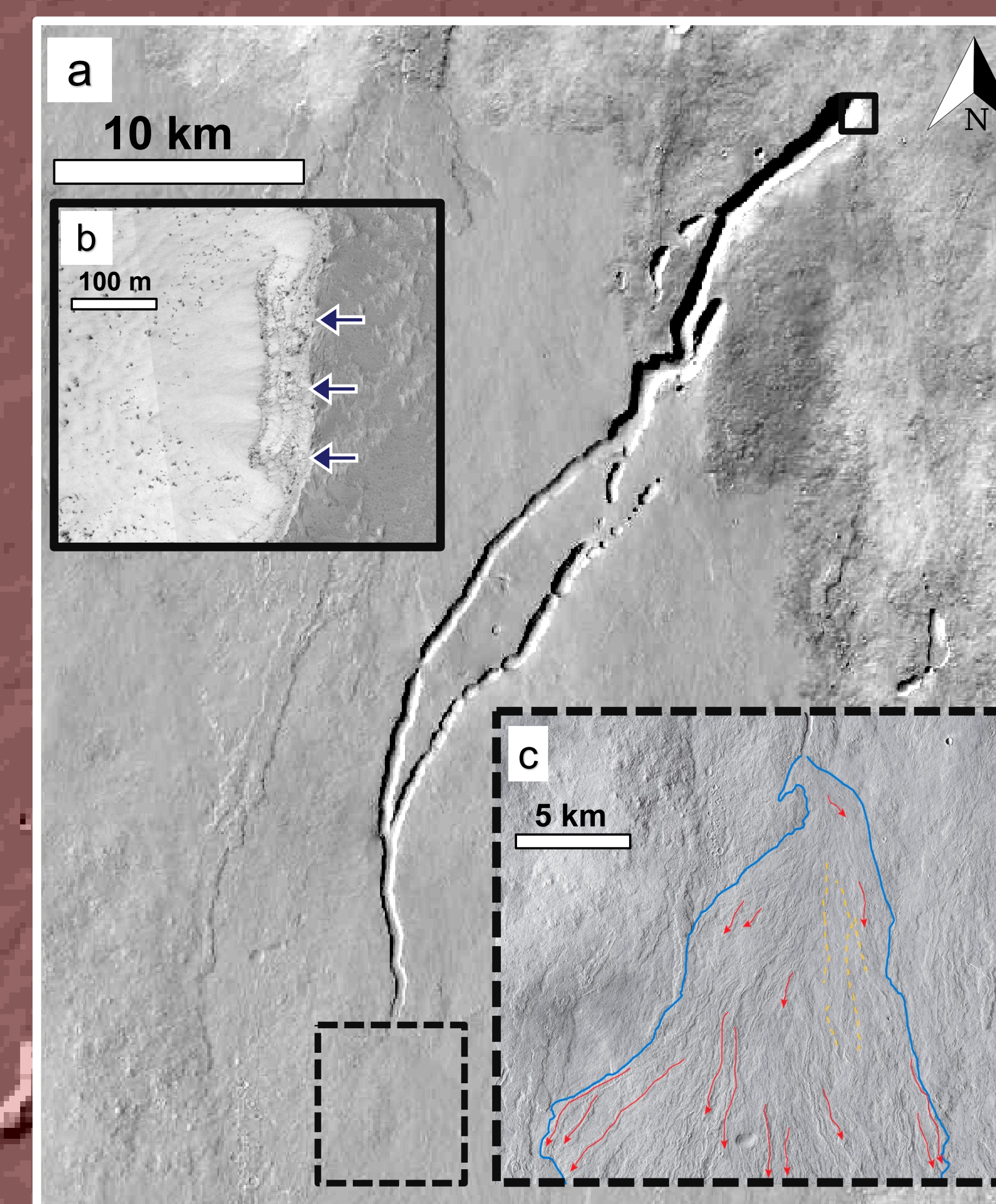


Figure 4: (a) CTX mosaic showing the potential source/vent for Flows 1, 2, 3, and 5 (feature is centered at 14.5°S, 237.5°E). The black solid and dashed line boxes indicate the regions shown in (b) and (c), respectively. (b) The layering along the rille wall (indicated by arrows) is similar to that seen in linear vents identified east of Arsia Mons [18]. (c) Lava fan emanating from the end of the rille structure (outlined by the blue line), which develops into a full flow field further south. The orange dashed lines indicate lava channels, and the red arrows denote lava flows.

Results

Step 1 Results: The modeled effusion rates, final flow viscosity, and final yield strength are summarized in Table 1. These effusion rates are an order of magnitude higher than recent terrestrial eruptions yet fall within the ranges from previous investigations of Arsia Mons lava flows [12-14] as well as for past large terrestrial eruptions [15].

Step 2 Results: The average channel width for the flows narrowed ~600% over the length of the exposed channels (Fig. 2). Assuming a narrowing rate further upslope, results for three of the flows (Flows 1, 3, and 5) project to the same feature (Fig. 3). Flow morphology and mapping also indicate that Flow 2 may originate from the same feature. We identify this as a long (~48 km) rille with a measured average width of ~873 m (Fig. 4). A lava fan emanates from its southern end that later develops into a full flow field further south, adding credence to a flow source location. The rille's location relative to Arsia Mons is also consistent with terrestrial rift-analogs such as Hawai'i, the Galapagos, and Tolbachik [16, 17, 19].

Conclusions

In this study, we applied a modified version of the PyFLOWGO model to five channelized flows southwest of Arsia Mons. With the flexibility of this model, we were able to first determine the effusion rates, lava viscosities, and then for three of these flows, a possible vent location. Our modeling indicates that these lava flows in the southwest Arsia Mons flow fields were emplaced with effusion rates an order of magnitude higher than those common for larger, modern terrestrial eruptions, but with similar viscosities and yield strengths. This study has shown that PyFLOWGO is an effective model to reproduce the emplacement conditions of planetary channelized flows.

Using the PyFLOWGO model and image analysis to identify possible vent locations, we plan to compile a more complete record of flow field evolution. Future applications of this approach include investigating the other flows around Arsia Mons, as well as those in Daedalia Planum, Elysium Mons, and the other Tharsis volcanoes.

Acknowledgments & References

This work was funded by a NASA Solar System Workings (SSW) grant (80NSSC19K0547).

- [1] Garry W. B. et al. (2007) JGR Planets, 112, 1-21. [2] Glaze L. S. & Baloga S. M. (2006) JGR Planets, 111, 1-10. [3] Hiesinger H. et al. (2007) JGR, 112, E05011, 24 pp. [4] Hodges C. A. & Moore H. J. (1994) Atlas of volcanic landforms on Mars, US Printing Office. [5] Crown D. A. & Ramsey M. S. (2017) JVGR, 342, 13-28. [6] Ramsey M. S. et al. (2019) Ann. Geophys, 62, 1-44. [7] Rowland S. K. et al. (2004) JGR Planets, 109, 1-16. [8] Rowland S. K. et al. (2005) Bull Volc 67, 634-647. [9] Cashman K. V. et al. (2013) Geosphere 9. [10] Dietterich H. R. & Cashman K. V. (2014) JGR ES 119, 1704-1724. [11] Peitersen M. & Crown D. A. (1999) JGR 104, 8473-8488. [12] Dvigalo V. N. et al. (2013) JVS, 7, 345-361. [13] Kubanek J. et al. (2017) JGR SE 122, 7754-7774. [14] Warner N. H. & Gregg T. K. P. (2003) JGR Planets 108. [15] Belousov A. & Belousova M. (2018) Bull Volc 80. [16] Rowland S. K. et al. (2002) LPSC XXXIII, Abstract #1441. [17] Bleacher J. E. et al. (2007) JGR Planets, 112, 1-15. [18] Hauber E. et al. (2009) JVGR 185, 69-95. [19] Mougins-Mark P. & Rowland S. K. (2001) Geomorph, 37, 201-223